

Learning tensor trains from noisy functions with application to quantum simulation

Kohtaroh Sakaue^{1*}
 Hiroshi Shinaoka¹
 Rihito Sakurai^{1,2}

¹ Department of Physics, Saitama University, Saitama 338-8570, Japan

² Department of Physics, The University of Tokyo, Tokyo 113-0033, Japan

* spikekohtaroh@gmail.com

May 22, 2024

Abstract

Tensor cross interpolation (TCI) is a powerful technique for learning a tensor train (TT) by adaptively sampling a target tensor based on an interpolation formula. However, when the tensor evaluations contain random noise, optimizing the TT is more advantageous than interpolating the noise. Here, we propose a new method that starts with an initial guess of TT and optimizes it using non-linear least-squares by fitting it to measured points obtained from TCI. We use quantics TCI (QTCI) in this method and demonstrate its effectiveness on sine and two-time correlation functions, with each evaluated with random noise. The resulting TT exhibits increased robustness against noise compared to the QTCI method. Furthermore, we employ this optimized TT of the correlation function in quantum simulation based on pseudo-imaginary-time evolution, resulting in ground-state energy with higher accuracy than the QTCI or Monte Carlo methods.

Contents

1	Introduction	2
2	Quantics tensor train	3
2.1	Tensor train	3
2.2	Quantics tensor train	4
2.2.1	Examples of QTT	5
3	Tensor train learning algorithm	5
3.1	Tensor cross interpolation	5
3.2	Singular value decomposition	5
4	Learning tensor trains from noisy functions	6
4.1	Outline	6
4.2	Demonstration	7
5	Application to quantum simulation based on pseudo-imaginary-time evolution	8
5.1	Setup	8

5.1.1	Imaginary-time evolution	8
5.1.2	Pseudo-imaginary-time evolution	9
5.1.3	Monte Carlo Method	10
5.1.4	Tensor network-based method	11
5.1.5	Ground-state energy calculations based on our proposed method	11
5.2	Numerical details	12
5.2.1	Software and hardware	12
5.2.2	Hamiltonian	12
5.2.3	Bond dimensions χ and $\tilde{\chi}$ in two-time correlation functions	13
5.2.4	Other parameters	13
5.3	Demonstration	13
6	Conclusion	15
A	Element-wise multiplication and integration with tensor trains	16
A.1	Element-wise multiplication	16
A.2	Integration	17
B	Calculating the real-time correlation function $\langle O \rangle(t, t')$	18
C	Bond dimensions of two-time correlation functions without noise	20
	References	20

1 Introduction

Tensor networks have emerged as a powerful technique for efficiently representing state vectors with exponentially large dimensions, originating from quantum many-body physics. In recent years, their applications have expanded to diverse fields, including image compression [1], machine learning [2, 3], solving partial differential equations [4–7], chemical master equation [8], quantum field theory [9–11], and finance [12, 13]. The success of tensor networks in these domains can be attributed to the inherent low-rank structure of the target tensors.

This hidden structure enables the efficient compression of high-dimensional tensor objects with numerous elements and computations using a key technique called tensor cross interpolation (TCI) [10, 14, 15]. TCI has proven to be an effective compression method that builds tensor trains (TTs) by adaptively sampling target tensors with a low-rank structure according to specific rules. Unlike singular value decomposition, which requires access to full tensors, TCI only needs a subset of the tensors, making it highly advantageous. TCI offers a promising approach for solving high-dimensional problems with low-rank structures and can potentially serve as an alternative to the Monte Carlo method.

However, when TCI is applied to tensors whose entries are affected by random noise during evaluation, its effectiveness becomes uncertain. This is because TCI interpolates the noise at the chosen points, leading to overfitting. This situation is particularly relevant in practical applications, such as quantum computing or Monte Carlo simulations, where statistical errors are unavoidable when measuring expectation values. In quantum com-

puting, which is the main application of this study, shot noise arises from the finite number of measurements needed to compute the expectation values of an observable. This noise can lead to inaccuracies in the tensor elements and subsequently affect the quality of the TT approximation obtained through TCI. Therefore, the presence of noise in tensor evaluations raises questions about the robustness and reliability of TCI in practical scenarios. A recent study [16] has investigated the effect of noise in TCI, while previous research has employed an error-mitigated technique such as supervised machine learning, using qubit measurement results as training data in quantum state tomography with TCI [17].

Here, we propose a new method for optimizing TTs that is more advantageous than interpolating noise on chosen tensors. Specifically, we start with an initial guess of TT and optimize it by fitting it to the measured points obtained from TCI by using the non-linear least-squares method. These measured points served for fitting collectively capture the global structure of the target function. This optimization process allows us to mitigate the effect of noise and get the optimized TT that correctly approximates noise-free functions. To demonstrate the effectiveness of our proposed method, we combine it with quantics TCI (QTCI) [18] and apply it to two different functions with continuous variables: a sine function and a two-time correlation function. In both cases, we show that our method achieves higher precision compared to the QTCI method (see Figs. 2 and 6). Finally, we apply our proposed method to quantum simulation based on pseudo-imaginary-time evolution for calculating the ground-state energy. Our proposed method yields a more accurate ground-state energy than those obtained using QTCI or Monte Carlo methods (see Fig. 5). Our results demonstrate that our proposed method enables robust learning TTs from functions under the influence of noise.

This paper is organized as follows: Section 2 introduces the TT. Section 3 introduces TCI for building TTs by adaptive sampling of target tensors. Section 4 introduces our proposed method for optimizing TTs for functions affected by random noise in function evaluations. Section 5 outlines the quantum simulation based on a pseudo-imaginary-time evolution algorithm for calculating the ground-state energy and results combined with our proposed method and compares results with conventional methods. Section 6 summarizes this study and discusses future directions.

2 Quantics tensor train

We introduce the TT and quantics tensor train (QTT) [19–21], suitable for compressing functions with continuous variables.

2.1 Tensor train

A tensor of dimension \mathcal{L} , $F_{\sigma_1\sigma_2\dots\sigma_{\mathcal{L}}}$, where each local index σ_l (for $l = 1, \dots, \mathcal{L}$) has local dimension d , can be decomposed into a TT. The TT representation is a type of tensor network with a one-dimensional structure. A TT decomposition is achieved by applying matrix decomposition techniques [14, 22]:

$$\begin{aligned} F_{\sigma_1\sigma_2\dots\sigma_{\mathcal{L}}} &\simeq \tilde{F}_{\sigma_1\sigma_2\dots\sigma_{\mathcal{L}}} \\ &= \sum_{\alpha_1=1}^{\chi_1} \cdots \sum_{\alpha_{\mathcal{L}-1}=1}^{\chi_{\mathcal{L}-1}} [F_1]_{1\alpha_1}^{\sigma_1} \cdots [F_l]_{\alpha_{l-1}\alpha_l}^{\sigma_l} \cdots [F_{\mathcal{L}}]_{\alpha_{\mathcal{L}-1}1}^{\sigma_{\mathcal{L}}} \\ &\equiv [F_1]_{\sigma_1} \cdots [F_l]_{\sigma_l} \cdots [F_{\mathcal{L}}]_{\sigma_{\mathcal{L}}}, \end{aligned} \quad (1)$$

where the third-order tensor $[F_l]_{\alpha_{l-1}\alpha_l}^{\sigma_l}$ has dimensions $\sigma_l \times \chi_{l-1} \times \chi_l$, where α_l is the virtual bond index with dimension χ_l , referred to as the bond dimension. The maximum bond

dimension is denoted by χ . If the bond dimension χ_l remains constant with increasing the number of tensors \mathcal{L} , the tensor $F_{\sigma_1\sigma_2\dots\sigma_{\mathcal{L}}}$ has a low-rank structure. The tilde in $\tilde{F}_{\sigma_1\sigma_2\dots\sigma_{\mathcal{L}}}$ indicates TT compression, and this notation is used hereafter.

2.2 Quantics tensor train

To introduce QTT, we consider a univariate function $f(x)$ defined on $x \in [0, 1)$. Here, we discretize the continuous variable x by setting up $d = 2^{\mathcal{R}}$ equally spaced grids on the x -axis. This discretization allows us to obtain a tensor representation of $f(x)$ as a vector F_{σ} with d elements indexed by σ :

$$F_{\sigma} = f(x(\sigma)). \quad (2)$$

In QTT, the discrete variable x is encoded in binary code:

$$x(\sigma_1, \dots, \sigma_{\mathcal{R}}) = \sum_{r=1}^{\mathcal{R}} \frac{\sigma_r}{2^r}, \quad \sigma_r \in \{0, 1\}, \quad (3)$$

where σ_r represents bits indicating different length scales 2^{-r} , and \mathcal{R} denotes the number of bits. Next, we reshape this vector F_{σ} into an \mathcal{R} -order tensor of $2 \times \dots \times 2$:

$$f(x) = f(x(\sigma_1\sigma_2, \dots, \sigma_{\mathcal{R}})) = F_{\sigma_1\sigma_2\dots\sigma_{\mathcal{R}}} = F_{\sigma}. \quad (4)$$

We assume that the correlation between significantly different length scales is weak. To take advantage of this weak correlation structure, we employ the TT decomposition, as defined in Eq. (1), to compress the tensor as follows:

$$F_{\sigma} = F_{\sigma_1\sigma_2\dots\sigma_{\mathcal{R}}} \approx \tilde{F}_{\sigma} = [F_1]_{\sigma_1} [F_2]_{\sigma_2} \cdots [F_{\mathcal{R}}]_{\sigma_{\mathcal{R}}}. \quad (5)$$

QTT can also be extended to a multivariate function $f(\mathbf{x})$ with real continuous variables $\mathbf{x} = (x_1, \dots, x_n)$ defined in $[0, 1)$. Each variable $x_l (l = 1, \dots, n)$ is discretized and encoded in binary code:

$$x_l(\sigma_{l1}, \dots, \sigma_{l\mathcal{R}}) = \sum_{r=1}^{\mathcal{R}} \frac{\sigma_{lr}}{2^r}, \quad \sigma_{lr} \in \{0, 1\}, \quad l = 1, \dots, n. \quad (6)$$

In multivariate functions, we perform scale separation, which involves arranging indices representing the same length scales to be adjacent. This yields an $n\mathcal{R}$ -order tensor F_{σ} of $f(\mathbf{x})$. We decompose F_{σ} as follows using TT decomposition:

$$\begin{aligned} F_{\sigma} &= F_{\sigma_{11}, \dots, \sigma_{n1}, \dots, \sigma_{1\mathcal{R}}\sigma_{n\mathcal{R}}} \\ &= f(x_1(\sigma_{11}, \dots, \sigma_{1\mathcal{R}}), x_2(\sigma_{21}, \dots, \sigma_{2\mathcal{R}}), \dots, x_n(\sigma_{n1}, \dots, \sigma_{n\mathcal{R}})) \\ &\simeq \tilde{F}_{\sigma} = [F_1]_{\sigma_{11}} \cdots [F_{n\mathcal{R}}]_{\sigma_{n\mathcal{R}}}. \end{aligned} \quad (7)$$

As a concrete case of a bivariate function $f(x, y)$ defined for normalized variables $x, y \in [0, 1)$, we decompose F_{σ} into \tilde{F}_{σ} as follows:

$$\begin{aligned} F_{\sigma} &= F_{\sigma_{11}, \sigma_{21}, \dots, \sigma_{1\mathcal{R}}\sigma_{2\mathcal{R}}} \\ &= f(x(\sigma_{11}, \dots, \sigma_{1\mathcal{R}}), y(\sigma_{21}, \dots, \sigma_{2\mathcal{R}})) \\ &\simeq \tilde{F}_{\sigma} = [F_1]_{\sigma_{11}} [F_2]_{\sigma_{21}} [F_3]_{\sigma_{12}} [F_4]_{\sigma_{22}} \cdots [F_{2\mathcal{R}-1}]_{\sigma_{1\mathcal{R}}} [F_{2\mathcal{R}}]_{\sigma_{2\mathcal{R}}}. \end{aligned} \quad (8)$$

2.2.1 Examples of QTT

For some analytic functions, their exact bond dimensions in QTT are known. The simplest example is an exponential function. For the exponential function $f(x) = e^{\lambda x}$, F_{σ} can be obtained in QTT as shown in Eq. (9):

$$F_{\sigma} = \prod_{l=1}^{\mathcal{R}} e^{\lambda \sigma_l / 2^l}, \quad (9)$$

where F_{σ} can be written as the direct product of $M_l = e^{\lambda \sigma_l / 2^l}$ ($l = 1, \dots, \mathcal{R}$), which indicates that the QTT has a exact bond dimension of 1.

For another example, the sine function $f(x) = \sin(\lambda x)$, being exactly equal to the subtraction of two exponential functions $e^{i\lambda x}$ and $e^{-i\lambda x}$, is known to have a bond dimension of 2 in QTT [20, 21].

3 Tensor train learning algorithm

We introduce a tensor train learning algorithm to build TTs from target tensors: tensor cross interpolation.

3.1 Tensor cross interpolation

Tensor cross interpolation (TCI) is a method for building a TT by adaptively sampling a subset of a tensor F_{σ} with a low-rank structure. TCI is particularly effective when the number of elements of the target tensor is substantially large because it only requires some tensor elements to build the TT. Thus, TCI adaptively selects sampling points to learn the tensor network, which can be regarded as active machine learning. In particular, combining QTT and TCI is called quantum tensor cross interpolation (QTTCI) [18], allowing for the efficient compression of functions with continuous variables and computations. TCI is a quasi-optimal algorithm in the maximum norm, as given by

$$\epsilon_{\text{TCI}} = \frac{|F_{\sigma} - \tilde{F}_{\text{TT}}|_{\max}}{|F_{\sigma}|_{\max}}, \quad (10)$$

where F_{σ} is the original function, and \tilde{F}_{TT} is the estimated TT obtained by TCI. The denominator is a normalization factor, which is the estimated absolute value of the function F_{σ} , denoted as $|F_{\sigma}|_{\max}$, and is used to handle cases where F_{σ} might include zero values for numerical stability. In this paper, we perform TCI by setting the maximum bond dimension of \tilde{F}_{TT} , instead of specifying a tolerance as in Eq. (10).

TCI is an interpolation formula, meaning that at the selected interpolation point σ , F_{σ} strictly matches \tilde{F}_{TT} as

$$\tilde{F}_{\text{TT}} = F_{\sigma}. \quad (11)$$

Here, we define measured points as the set of all indices and corresponding tensor values sampled during the execution of TCI. Interpolation points are a subset of these measured points used to build the TT through TCI.

3.2 Singular value decomposition

In this study, we use singular value decomposition (SVD) to reduce further the bond dimension of TTs obtained from TCI. SVD can decompose a given TT into another TT

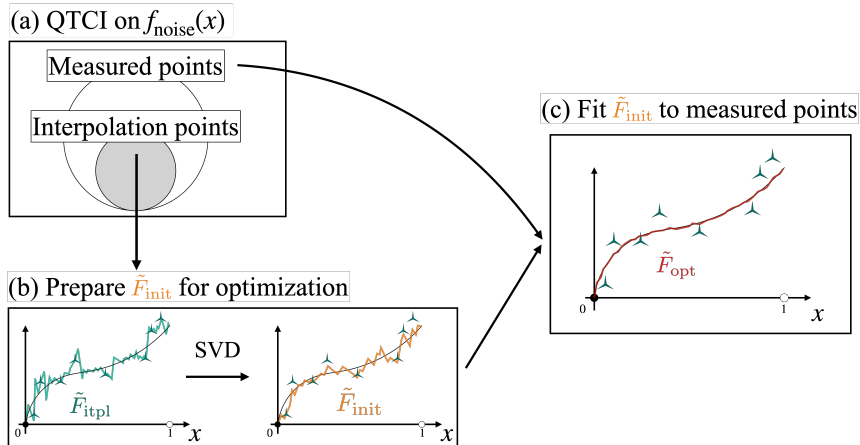


Figure 1: The optimization of TTs proposed in this study. In Step (a), we apply the QTCI to the function $f_{\text{noise}}(\mathbf{x})$ evaluated with random noise and store measured points obtained from QTCI. In Step (b), we build \tilde{F}_{itpl} , which is composed of interpolation points obtained from QTCI, where the triangle marks in (b) represent the interpolation points. This is then compressed by applying SVD to obtain an initial guess of QTT, \tilde{F}_{init} . In Step (c), we optimize the \tilde{F}_{init} by fitting it to the measured points obtained in Step (a) by applying the least squares method to reduce the effect of noise in \tilde{F}_{init} . This results in \tilde{F}_{opt} that approximate the noise-free function $f(\mathbf{x})$.

with an optimal rank in terms of the Frobenius norm, using a given error tolerance ϵ_{SVD} . This tolerance is defined by

$$\epsilon_{\text{SVD}} = \frac{|\tilde{F}_{\text{TT}} - \tilde{F}'_{\text{TT}}|_{\text{F}}^2}{|\tilde{F}_{\text{TT}}|_{\text{F}}^2}, \quad (12)$$

where $|\cdots|_{\text{F}}^2$ indicates the Frobenius norm, \tilde{F}_{TT} is the TT obtained from TCI and \tilde{F}'_{TT} is the other TT after SVD. In this paper, we perform SVD by setting the maximum bond dimension of \tilde{F}'_{TT} .

4 Learning tensor trains from noisy functions

We propose a method for optimizing TTs for functions affected by random noise in function evaluations. Here, we optimize an initial guess of TT by fitting it to measured points obtained from TCI, which capture the global structure of the target functions. This optimization yields the optimized TT that accurately approximates the noise-free function. Especially for functions with continuous variables, we use the QTCI in our proposed methods. We demonstrate our approach with a simple sin function example. More challenging examples, such as cases where the bond dimension is not exactly known, will be introduced in the next section.

4.1 Outline

Step (a) Perform QTCI to learn \tilde{F}_{itpl} from a function $f_{\text{noise}}(\mathbf{x})$ that is subject to random noise during evaluation, setting the maximum bond dimension of QTCI to $\tilde{\chi}$. At the same time, we store all the results of function evaluations on the measured points obtained from QTCI shown in Fig. 1(a).

Step (b) Prepare the initial guess \tilde{F}_{init} for optimization by compressing \tilde{F}_{itpl} from maximum bond dimension $\tilde{\chi}$ to χ ($\chi \leq \tilde{\chi}$) using SVD shown in Fig. 1(b).

Step (c) Starting from the initial guess \tilde{F}_{init} obtained in Step (b), we fit this TT to the measured points using the non-linear least-squares method shown in Fig. 1(c). As a result, we get optimized TT, \tilde{F}_{opt} that approximate the noise-free function $f(\mathbf{x})$.

Each of these Steps is explained in more detail below.

First, in Step (a), we learn the QTT, \tilde{F}_{itpl} from the multivariable function $f_{\text{noise}}(\mathbf{x})$ evaluated with random noise using QTCI, setting the maximum bond dimension of QTCI to $\tilde{\chi}$. Note that \tilde{F}_{itpl} strictly interpolates the noise at points adaptively sampled by QTCI. At the same time, we record the measured points obtained from QTCI, whose number is N^{TCI} . This measured point captures the global structure of the original noise-free function $f(\mathbf{x})$, and we utilize them for fitting in optimization. The bond dimension $\tilde{\chi}$ specified in the QTCI is a hyperparameter.

In Step (b), we employ SVD to reduce the maximum bond dimension of \tilde{F}_{itpl} from $\tilde{\chi}$ to a smaller value χ , which is treated as a hyperparameter. This truncation process yields a new QTT, denoted as \tilde{F}_{init} , which serves as the initial guess for the subsequent fitting process. The procedure for setting the hyperparameters χ and $\tilde{\chi}$ is discussed in Sec. 5.2.3.

In Step (c), we start with \tilde{F}_{init} obtained in Step (b) and fit it to the measured points saved in Step (a) to reduce the effect of noise in \tilde{F}_{init} . That is, we optimize the variational parameters, which correspond to each element of \tilde{F}_{init} , to minimize the following cost function using non-linear least-squares:

$$\text{cost}(\mathbf{z}) \equiv \sum_{i=1}^{N^{\text{TCI}}} |z_i - z'_i|^2, \quad (13)$$

where z_i ($i = 1, \dots, N^{\text{TCI}}$) denote the values of the N^{TCI} measured points. Furthermore, z'_i ($i = 1, \dots, N^{\text{TCI}}$) represent the values of \tilde{F}_{init} with indices of z_i . We denote the number of optimizations performed during fitting as n_{itr} . After optimization, we get the optimized TT that accurately approximates the noise-free function.

4.2 Demonstration

As a simple demonstration, we consider the sine function $f(x) = \sin(2\pi x)$ defined over the interval $x \in [0, 1)$. We add Gaussian noise in the form of a normal distribution $N(\mu, \sigma^2)$ with mean μ and standard deviation σ , resulting in the function $f_{\text{noise}}(x, \mu, \sigma) = f(x) \times (1 + N(\mu, \sigma^2))$.

The numerical details are as follows. We set $\mathcal{R} = 12$, the mean of the normal distribution $\mu = 0$, $\tilde{\chi} = 6$, and $\chi = 2$. The choice of $\chi = 2$ is based on the exact bond dimension required for representing $f(x) = \sin(2\pi x)$ in QTT, while $\tilde{\chi} = 6$ is selected to larger value in order to increase the number of fitting points which capture the global structure of the target function. Also, we set the number of fitting iterations $n_{\text{itr}} = 500$. This number was set after observing the decrease in the cost function during iterations, ensuring that the cost function converged sufficiently and remained nearly constant. We repeated this procedure 20 times using different realizations of noise.

Figure. 2(a) shows results for $\sigma = 0.1$. Our proposed method not only brings the mean values closer to those of the noise-free function but also reduces the variance. Furthermore, the results for absolute error demonstrate that the proposed method reduces the average effect of noise on the function in terms of absolute error.

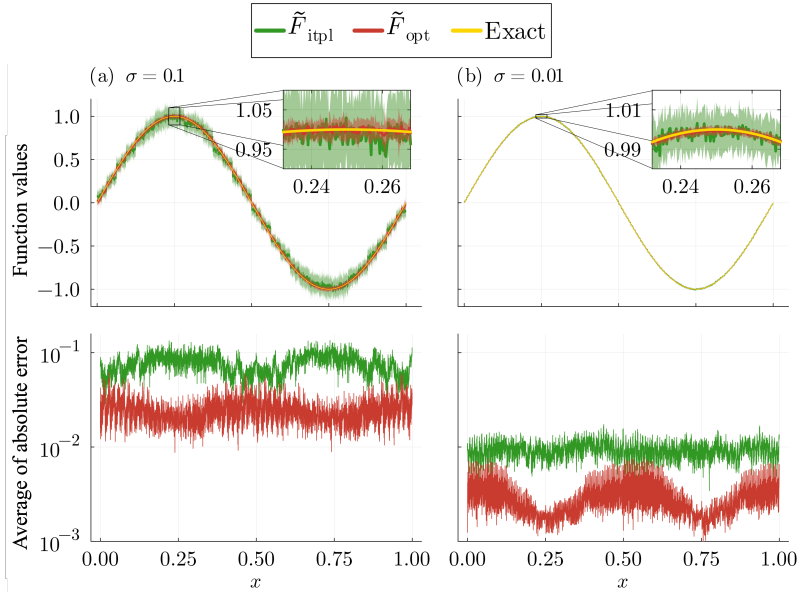


Figure 2: Results for our method applied to $f_{\text{noise}}(x, \mu, \sigma) = f(x) \times (1 + N(\mu, \sigma^2))$ with standard deviations of the normal distribution $\sigma = 0.1$ and $\sigma = 0.01$ are shown in (a) and (b), respectively. The upper part panel shows the mean and variance of 20 runs, and the lower panel shows the mean of the absolute error. The small figures inside the plots in the upper panel are enlarged views of the region around $x = 0.25$. \tilde{F}_{itpl} is the QTT from QTCl, \tilde{F}_{opt} the optimized QTT, and “Exact” the noise-free $f(x)$.

Figure 2(b) shows results for smaller $\sigma = 0.01$. One can see that, even with a further reduction of the noise effect, both variance and absolute error have been reduced by the proposed method.

5 Application to quantum simulation based on pseudo-imaginary-time evolution

5.1 Setup

We use our proposed method to learn QTTs of two-time correlation functions, calculated on a quantum computer, where noise such as Trotter error and shot noise are included. We then apply these optimized QTTs to quantum simulation based on pseudo-imaginary-time evolution to robustly compute the ground-state energy. For details on this pseudo-imaginary-time evolution method, please refer to Ref. [23].

5.1.1 Imaginary-time evolution

Using the traceless Hamiltonian \bar{H} (where $\text{Tr}(\bar{H}) = 0$) and a parameter E_0 , we redefine the Hamiltonian as $H = \bar{H} - E_0 \mathbb{I}$. Let E_g be the ground-state energy of \bar{H} obtained through exact diagonalization. The parameter E_0 is a hyperparameter necessary for determining the ground-state energy. Now, let β be the imaginary-time, $|\Psi(0)\rangle$ the initial state, and O a physical quantity. In the imaginary-time evolution method, the expectation value of

the physical quantity O at time β , denoted as $\langle O \rangle(\beta)$, is calculated as:

$$\langle O \rangle(\beta) = \frac{\langle \Psi(0) | e^{-\beta H} O e^{-\beta H} | \Psi(0) \rangle}{\langle \Psi(0) | e^{-2\beta H} | \Psi(0) \rangle} \equiv \frac{\langle O \rangle(-i\beta, i\beta)}{\langle 1 \rangle(-i\beta, i\beta)}, \quad (14)$$

where 1 represents the identity operator. In particular, if $O = \bar{H}$, the energy expectation value $\langle \bar{H} \rangle(\beta)$, calculated via the imaginary-time evolution method, is known to converge to the ground-state energy E_g of \bar{H} as β approaches infinity:

$$\lim_{\beta \rightarrow \infty} \langle \bar{H} \rangle(\beta) = E_g. \quad (15)$$

However, as the size of the system increases, the size of \bar{H} and H when represented as matrices also grow exponentially, making the calculations in Eqs. (14) and (15) difficult. To perform this imaginary-time evolution, several quantum algorithms have been proposed to approximate it using unitary operators, enabling its implementation on quantum computers [23–26].

5.1.2 Pseudo-imaginary-time evolution

We review the formalism based on Ref. [23]. We approximate the imaginary-time evolution operator $e^{-\beta H}$ by using the real-time evolution operator e^{-iHt} as follows:

$$e^{-\beta H} \approx G(H) = \int_{-\infty}^{\infty} dt g(t) e^{-iHt}, \quad (16)$$

where

$$g(t) = f_L(\beta, t) \cdot f_G(1, 0, \tau, \sqrt{\beta^2 + t^2}) = \frac{1}{\pi} \frac{\beta}{\beta^2 + t^2} e^{-\frac{\beta^2 + t^2}{2\tau^2}}, \quad (17)$$

where $g(t)$ is the product of Lorentz and Gaussian functions. The Lorentz function is $f_L(\beta, t) = \frac{1}{\pi} \frac{\beta}{\beta^2 + t^2}$, and the Gaussian function is $f_G(A, \mu, \sigma, x) = A \exp\left(-\frac{(x-\mu)^2}{2\sigma^2}\right)$. The parameter τ corresponds to the standard deviation of the Gaussian function. In the following, we refer to this method as pseudo-imaginary-time evolution.

Using the complementary error function, $\text{erfc}(x) = \frac{2}{\sqrt{\pi}} \int_x^{\infty} e^{-t^2} dt$ and the eigenvalues ω of H , Eq. (16) can be written as

$$G(\omega) = \sum_{\eta=\pm} \frac{1}{2} e^{\eta\beta\omega} \text{erfc}\left(\frac{\beta + \eta\omega\tau^2}{\sqrt{2}\tau}\right). \quad (18)$$

Here, the error in Eq. (16) is bounded using the matrix2-norm ($\|\cdot\|_2$) when H is positive semidefinite, i.e., when $\Delta E = E_g - E_0 \geq \frac{\beta}{\tau^2}$, as follows:

$$\|G(H) - e^{-\beta H}\|_2 \leq \gamma_G = e^{-\frac{\Delta E^2 \tau^2}{2}}. \quad (19)$$

Next, the expectation value of the physical quantity O , $\langle O \rangle(\beta)$, can be approximated by replacing the imaginary-time evolution $e^{-\beta H}$ with Eq. (16) and thus translated into an integral calculation using the real-time evolution operator:

$$\langle O \rangle_G(\beta) = \frac{\langle O \rangle_G(-i\beta, i\beta)}{\langle 1 \rangle_G(-i\beta, i\beta)}, \quad (20)$$

$$\langle O \rangle_G(-i\beta, i\beta) = \langle \Psi(0) | G(H) O G(H) | \Psi(0) \rangle = \int dt dt' g(t) g(t') \langle O \rangle(t, t'), \quad (21)$$

$$\begin{aligned} \langle O \rangle(t, t') &= \langle \Psi(0) | e^{iHt'} O e^{-iHt} | \Psi(0) \rangle = e^{iE_0(t-t')} \langle \Psi(0) | e^{i\bar{H}t'} O e^{-i\bar{H}t} | \Psi(0) \rangle \\ &= e^{iE_0(t-t')} \overline{\langle O \rangle}(t, t'), \end{aligned} \quad (22)$$

where $\overline{\langle O \rangle}(t, t')$ is denoted as $\langle \overline{O} \rangle(t, t')$.

Next, we consider replacing the infinite integration range with a finite one T in Eq. (16) as

$$G_T(H) = \int_{-T}^T dt g(t) e^{-iHt}. \quad (23)$$

The error between $G(H)$ and $G_T(H)$ is given by

$$\|G_T(H) - G(H)\|_2 \leq \gamma_T = \frac{\sqrt{2}\tau}{\sqrt{\pi}\beta} e^{-\frac{T^2}{2\tau^2}}. \quad (24)$$

Using Eq. (23), the finite integration range versions of Eqs. (20) and (21) are defined as follows:

$$\langle O \rangle_{G_T}(\beta) = \frac{\langle O \rangle_{G_T}(-i\beta, i\beta)}{\langle 1 \rangle_{G_T}(-i\beta, i\beta)}, \quad (25)$$

$$\langle O \rangle_{G_T}(-i\beta, i\beta) = \langle \Psi(0) | G_T(H) O G_T(H) | \Psi(0) \rangle = \int_{-T}^T dt dt' g(t) g(t') \langle O \rangle(t, t'), \quad (26)$$

where the integration range T and the constant E_0 are crucial parameters related to the accuracy of the expected value $\langle O \rangle$. The optimal selection of these parameters is beyond the scope of this study. In this research, the parameters are fixed as stated in Sec. 5.2.4, and their sufficiency for achieving adequate accuracy is verified.

We consider calculating the ground-state energy $\langle \bar{H} \rangle(\beta)$ of a given Hamiltonian \bar{H} (where $O = \bar{H}$):

$$E_g \sim \langle \bar{H} \rangle(\beta) \simeq \langle \bar{H} \rangle_{G_T}(\beta) = \frac{\langle \bar{H} \rangle_{G_T}(-i\beta, i\beta)}{\langle 1 \rangle_{G_T}(-i\beta, i\beta)}. \quad (27)$$

5.1.3 Monte Carlo Method

This section describes a simplified version of the quantum algorithm from [23] for calculating the expectation value $\langle O \rangle_{G_T}(-i\beta, i\beta)$ in Eq. (26) using the Monte Carlo method. The method involves independently sampling times t and t' from probability density functions $g(t)$ and $g(t')$ within $[-T, T]$, and evaluating the expectation value by measuring the two-point real-time correlation function $\langle O \rangle(t, t')$ at the sampled times on a quantum computer. The expectation value is given by:

$$\langle O \rangle_{G_T}(-i\beta, i\beta) = C^2 \int_{-T}^T dt dt' P(t, t') \langle O \rangle(t, t') \sim \frac{C^2}{N^{\text{MC}}} \sum_{i=1}^{N^{\text{MC}}} \langle O \rangle(t_i, t'_i). \quad (28)$$

where $C = \int_{-T}^T dt g(t) = \int_{-T}^T dt' g(t')$ is the normalization constant, and $P(t, t') = \frac{g(t)g(t')}{C^2}$ is the product of the independent probability density functions. The Monte Carlo method converges to the desired expectation value at a rate of $\mathcal{O}\left(\frac{1}{\sqrt{N^{\text{MC}}}}\right)$ with respect to the number of samples N^{MC} .

5.1.4 Tensor network-based method

The $\langle O \rangle_{G_T}(-i\beta, i\beta)$ can be directly calculated using QTT as follows:

$$\begin{aligned} \langle O \rangle_{G_T}(-i\beta, i\beta) &= \int_{-T}^T dt dt' e^{iE_0(t-t')} g(t) g(t') \langle \Psi(0) | e^{i\tilde{H}t'} O e^{-i\tilde{H}t} | \Psi(0) \rangle \\ &= \int_{-T}^T dt dt' E(E_0, t, t') G(t, t') \overline{\langle O \rangle}(t, t') \\ &\simeq \langle \tilde{O} \rangle_{G_T}(-i\beta, i\beta) \end{aligned} \quad (29)$$

where $E(E_0, t, t') = e^{iE_0(t-t')}$, $G(t, t') = g(t)g(t')$, and $\overline{\langle O \rangle}(t, t') = \langle \Psi(0) | e^{i\tilde{H}t'} O e^{-i\tilde{H}t} | \Psi(0) \rangle$. Each QTT is represented as $\tilde{E}_{t_1, t'_1, \dots, t_{\mathcal{R}}, t'_{\mathcal{R}}}$, $\tilde{G}_{t_1, t'_1, \dots, t_{\mathcal{R}}, t'_{\mathcal{R}}}$, and $\overline{\langle O \rangle}_{t_1, t'_1, \dots, t_{\mathcal{R}}, t'_{\mathcal{R}}}$, respectively. Using QTTs, the calculation of $\langle \tilde{O} \rangle_{G_T}(-i\beta, i\beta)$ that approximate $\langle O \rangle_{G_T}(-i\beta, i\beta)$ involves the following four Steps for a given value of E_0 (see Fig. 3):

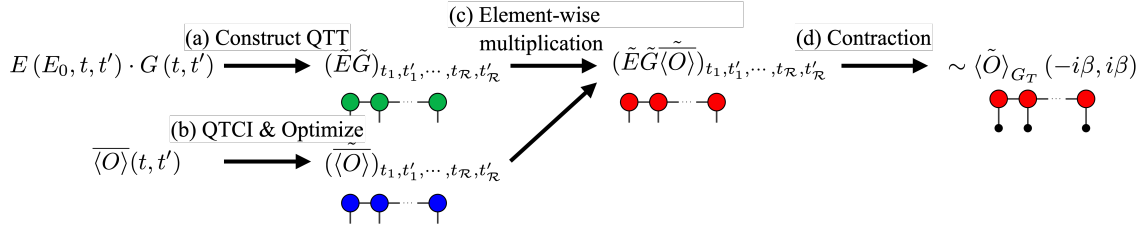


Figure 3: Calculating $\langle \tilde{O} \rangle_{G_T}(-i\beta, i\beta)$ using our proposed method through following Steps. First, in Step (a), we construct $(\tilde{E}\tilde{G})_{t_1, t'_1, \dots, t_{\mathcal{R}}, t'_{\mathcal{R}}}$ using the QTCI method. Next, in Step (b), we apply our proposed method to $\overline{\langle O \rangle}(t, t')$. Then, in Step (c), we perform element-wise multiplication of the QTTs obtained in Steps (a) and (b), resulting in $(\tilde{E}\tilde{G}\overline{\langle O \rangle})_{t_1, t'_1, \dots, t_{\mathcal{R}}, t'_{\mathcal{R}}}$. Finally, in Step (d), we integrate $(\tilde{E}\tilde{G}\overline{\langle O \rangle})_{t_1, t'_1, \dots, t_{\mathcal{R}}, t'_{\mathcal{R}}}$ over the range of $[-T, T]$ to compute $\langle \tilde{O} \rangle_{G_T}(-i\beta, i\beta)$.

- Step (a) Learn $\tilde{G}_{t_1, t'_1, \dots, t_{\mathcal{R}}, t'_{\mathcal{R}}}$ using QTCI. Then, we perform element-wise multiplication of $\tilde{E}_{t_1, t'_1, \dots, t_{\mathcal{R}}, t'_{\mathcal{R}}}$ with exact bond dimension and $\tilde{G}_{t_1, t'_1, \dots, t_{\mathcal{R}}, t'_{\mathcal{R}}}$ to construct the $(\tilde{E}\tilde{G})_{t_1, t'_1, \dots, t_{\mathcal{R}}, t'_{\mathcal{R}}}$. Details of the element-wise multiplication of QTTs are described in Appendix A.
- Step (b) Learn $\overline{\langle O \rangle}_{t_1, t'_1, \dots, t_{\mathcal{R}}, t'_{\mathcal{R}}}$ using our proposed method. Here, each element of the correlation function is computed using quantum computers, which introduces errors such as Trotter error and shot noise.
- Step (c) Perform element-wise multiplication of $(\tilde{E}\tilde{G})_{t_1, t'_1, \dots, t_{\mathcal{R}}, t'_{\mathcal{R}}}$ and $\overline{\langle O \rangle}_{t_1, t'_1, \dots, t_{\mathcal{R}}, t'_{\mathcal{R}}}$, which are obtained in Steps (a) and (b) respectively. As a result, we obtain $(\tilde{E}\tilde{G}\overline{\langle O \rangle})_{t_1, t'_1, \dots, t_{\mathcal{R}}, t'_{\mathcal{R}}}$ that approximate the $E(E_0, t, t') \cdot G(t, t') \cdot \overline{\langle O \rangle}(t, t')$.
- Step (d) Perform integration over the range $[-T, T]$ for the $(\tilde{E}\tilde{G}\overline{\langle O \rangle})_{t_1, t'_1, \dots, t_{\mathcal{R}}, t'_{\mathcal{R}}}$ obtained in Step (c) to calculate the integral value of $\langle \tilde{O} \rangle_{G_T}(-i\beta, i\beta)$. For more information on how TTs and integration are related, please refer to Appendix A.

5.1.5 Ground-state energy calculations based on our proposed method

We repeat four Steps in Sec. 5.1.4 while varying the value of E_0 over the range $[\tilde{E}_g - E, \tilde{E}_g + E]$ with step size N_{E_0} included in $\langle \tilde{O} \rangle_{G_T}(-i\beta, i\beta)$, the ground-state energy can be

determined as the minimal value (see Algorithm 1). Here, \tilde{E}_g is set close to the ground-state energy E_g obtained through mean-field approximation or similar techniques. In this study, we set $\tilde{E}_g = E_g$ and $E = 2$ as shown in Table 1.

Algorithm 1 Ground-state energy solver based on tensor trains

Require: $\tilde{H}, \tilde{E}_g, E, \beta, \tau, T, \mathcal{R}, \tau_{\text{TCI}}, \tilde{\chi}, \chi, n_{\text{itr}}, N_t, M_s$.

- 1: Prepare $\tilde{G}_{t_1, t'_1, \dots, t_{\mathcal{R}}, t'_{\mathcal{R}}}$ using the QTCI according to \mathcal{R} and τ_{TCI} .
 - 2: Learn $\langle \tilde{\tilde{H}} \rangle_{t_1, t'_1, \dots, t_{\mathcal{R}}, t'_{\mathcal{R}}}$ using our proposed method based on $\mathcal{R}, \tilde{\chi}, \chi, n_{\text{itr}}$.
 - 3: Take element-wise multiplication of $\tilde{G}_{t_1, t'_1, \dots, t_{\mathcal{R}}, t'_{\mathcal{R}}}$ and $\langle \tilde{\tilde{H}} \rangle_{t_1, t'_1, \dots, t_{\mathcal{R}}, t'_{\mathcal{R}}}$ to obtain $(\tilde{G}\langle \tilde{\tilde{H}} \rangle)_{t_1, t'_1, \dots, t_{\mathcal{R}}, t'_{\mathcal{R}}}$.
 - 4: Learn $\langle \tilde{\tilde{I}} \rangle_{t_1, t'_1, \dots, t_{\mathcal{R}}, t'_{\mathcal{R}}}$ using our proposed method based on $\mathcal{R}, \tilde{\chi}, \chi, n_{\text{itr}}$.
 - 5: Take element-wise multiplication of $\tilde{G}_{t_1, t'_1, \dots, t_{\mathcal{R}}, t'_{\mathcal{R}}}$ and $\langle \tilde{\tilde{I}} \rangle_{t_1, t'_1, \dots, t_{\mathcal{R}}, t'_{\mathcal{R}}}$ to obtain $(\tilde{G}\langle \tilde{\tilde{I}} \rangle)_{t_1, t'_1, \dots, t_{\mathcal{R}}, t'_{\mathcal{R}}}$.
 - 6: **for** $E_0 = \tilde{E}_g - E$ to $\tilde{E}_g + E$ with step size N_{E_0} **do**
 - 7: Build $\tilde{E}_{t_1, t'_1, \dots, t_{\mathcal{R}}, t'_{\mathcal{R}}}$ with exact bond dimension.
 - 8: Take element-wise multiplication of $\tilde{E}_{t_1, t'_1, \dots, t_{\mathcal{R}}, t'_{\mathcal{R}}}$ and $(\tilde{G}\langle \tilde{\tilde{H}} \rangle)_{t_1, t'_1, \dots, t_{\mathcal{R}}, t'_{\mathcal{R}}}$ to build $(\tilde{E}\tilde{G}\langle \tilde{\tilde{H}} \rangle)_{t_1, t'_1, \dots, t_{\mathcal{R}}, t'_{\mathcal{R}}}$ and store the integral value of $\langle \tilde{\tilde{H}} \rangle_{G_T}(E_0)$ obtained by integrating $(\tilde{E}\tilde{G}\langle \tilde{\tilde{H}} \rangle)_{t_1, t'_1, \dots, t_{\mathcal{R}}, t'_{\mathcal{R}}}$ over the range of $[-T, T]$.
 - 9: Take element-wise multiplication of $\tilde{E}_{t_1, t'_1, \dots, t_{\mathcal{R}}, t'_{\mathcal{R}}}$ and $(\tilde{G}\langle \tilde{\tilde{I}} \rangle)_{t_1, t'_1, \dots, t_{\mathcal{R}}, t'_{\mathcal{R}}}$ to build $(\tilde{E}\tilde{G}\langle \tilde{\tilde{I}} \rangle)_{t_1, t'_1, \dots, t_{\mathcal{R}}, t'_{\mathcal{R}}}$ and store the integral value $\langle \tilde{\tilde{I}} \rangle_{G_T}(E_0)$ obtained by integrating $(\tilde{E}\tilde{G}\langle \tilde{\tilde{I}} \rangle)_{t_1, t'_1, \dots, t_{\mathcal{R}}, t'_{\mathcal{R}}}$ over the range of $[-T, T]$.
 - 10: **end for**
 - 11: Define $\hat{E}(E_0) = \langle \tilde{\tilde{H}} \rangle_{G_T}(E_0) / \langle \tilde{\tilde{I}} \rangle_{G_T}(E_0)$.
- Ensure:** $\min_{E_0} \hat{E}(E_0) \leftarrow$ estimated ground-state energy
-

5.2 Numerical details

5.2.1 Software and hardware

We used `TensorCrossInterpolation.jl` for TCI [27], and `ITensors.jl` [28] for tensor contractions and SVD. We used `Kyulacs.jl` [29], a julia wrapper for `Qulacs` [30]. For the fitting TTs in our proposed method, the automatic differentiation and LBFGS optimization algorithm was used via `Optim.jl` [31], and `Zygote.jl` [32]. In our calculations, we used AMD EPYC 7702P 64-Core Processor. The total computation time for the largest system in this simulation, with 6 sites, was about 19 hours on a single CPU core.

5.2.2 Hamiltonian

For ground-state energy calculations, we consider the one-dimensional transverse-field Ising model Hamiltonian \tilde{H} :

$$\tilde{H} = - (2 - \lambda) \sum_{\langle i, j \rangle} \sigma_i^z \sigma_j^z - \lambda \sum_i \sigma_i^x, \quad (30)$$

where σ^z and σ^x are the Pauli-Z and Pauli-X operators, respectively. The model parameters include the number of sites n_{site} and the strength of the transverse field λ .

5.2.3 Bond dimensions χ and $\tilde{\chi}$ in two-time correlation functions

Since the exact bond dimensions of the two-time correlation function are unknown, we apply QTCI on this function evaluated with noise to estimate the χ and $\tilde{\chi}$ roughly.

Figures 4(a) and (b) show interpolation errors estimated by QTCI normalized by the estimated absolute values of the functions, ϵ_{TTCI} . The error ϵ_{TTCI} of QTCI initially decreases rapidly with increasing maximum bond dimension in the numerator and denominator, respectively. However, as $\tilde{\chi}$ increases, the error decrease stagnates, likely due to QTCI overfitting the noisy function evaluations, compromising approximation accuracy.

Based on this observation, we set $\tilde{\chi}$ to a value in the plateau region where ϵ_{TTCI} saturates in the presence of noise. Specifically, we set $\tilde{\chi} = 4, 6, 10$ for $n_{\text{site}} = 2, 4, 6$, respectively. Next, we choose χ based on the fact that a noiseless function can be represented with a smaller bond dimension, whereas a function with noise requires a larger bond dimension. In particular, we set $\chi = 2, 4, 8$ for $n_{\text{site}} = 2, 4, 6$, respectively. After selecting these bond dimensions, we confirm that the precision of the ground-state energy is maintained. The values of χ are reasonable based on the results of the noise-free two-time function in Appendix. C.

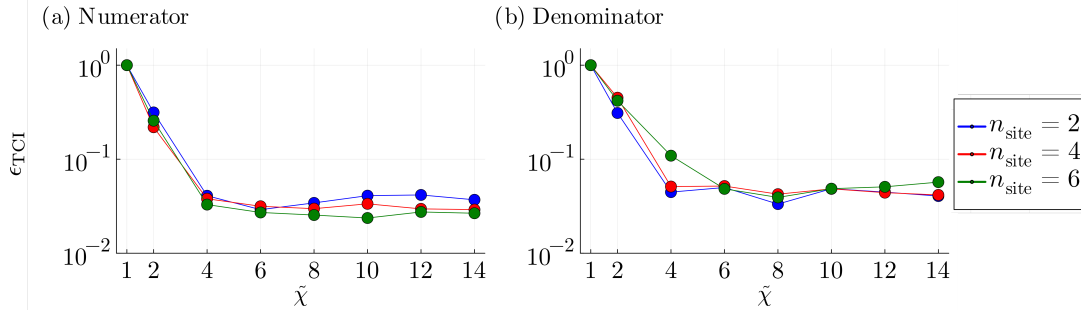


Figure 4: Normalized error ϵ_{TTCI} as a function of the bond dimension $\tilde{\chi}$ for QTCI. (a) numerator $\langle \bar{H} \rangle(t, t')$, and (b) denominator $\langle \bar{I} \rangle(t, t')$. The parameters such as λ , β , τ , T , \mathcal{R} , N_t , and M_s are set as in Table 1.

5.2.4 Other parameters

The parameters required to calculate the expectation value $\langle O \rangle_{G_T}(-i\beta, i\beta)$ are imaginary-time β , parameter τ , integration range T , the number of bits \mathcal{R} , the tolerance of the QTCI τ_{TTCI} , the number of Trotter step N_t and the number of measurement M_s for computing the correlation function $\langle \bar{O} \rangle(t, t')$ on a quantum simulator and the number of the optimization iterations n_{itr} . At the stage of tuning the E_0 to calculate the ground-state energy, its range E and step size N_{E_0} are also needed. These parameters are uniformly applied regardless of the size n_{site} as follows:

λ	β	τ	T	\mathcal{R}	τ_{TTCI}	N_t	M_s	n_{itr}	E	N_{E_0}
1.2	1.0	2.0	2.0	8	10^{-5}	100	15000	500	2	40

Table 1: Parameters used in the simulation.

5.3 Demonstration

Figure 5 shows the results of learning $\langle \tilde{O} \rangle_{t_1, t'_1, \dots, t_{\mathcal{R}}, t'_{\mathcal{R}}}$ using the proposed method under the influence of noise, i.e., shot noise and Trotter errors. These errors arise while using

quantum computers to evaluate each measured point of the two-time correlation function. We compare the results obtained using the QTCI method and the proposed method for estimating the correlation function $\langle \tilde{O} \rangle(t, t')$ in QTT. This demonstrates that the proposed approach effectively mitigates the impact of noise, resulting in enhanced accuracy of two-time correlation functions.

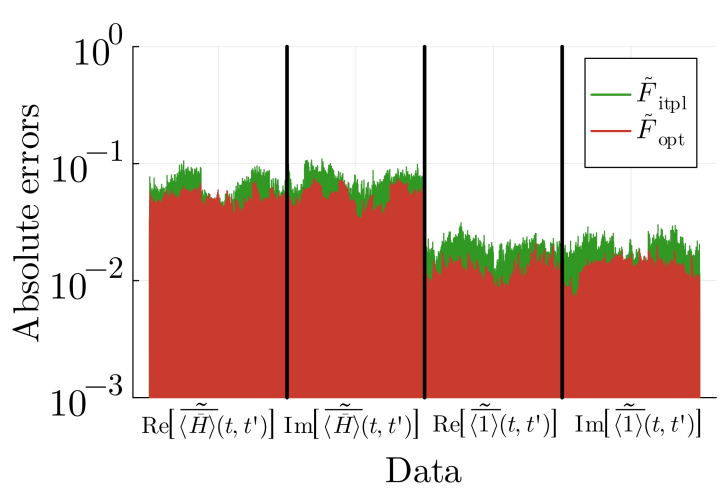


Figure 5: Results for the average absolute error between each of the values of the correlation function $\langle \tilde{H} \rangle(t, t')$ and $\langle \tilde{I} \rangle(t, t')$ obtained by applying the QTCI method (denoted as \tilde{F}_{itpl}) or the proposed method (denoted as \tilde{F}_{opt}) and the values from state vector simulation without noise. The average absolute error was calculated over 20 trials, each using a different set of random numbers. The presented results include the one-dimensional reshaped data series of function values that depend on t and t' . In both methods, for a system size of $n_{\text{site}} = 4$, the parameters such as λ , β , τ , T , \mathcal{R} , N_t , and M_s defined in Table 1 were used.

Then, we move on to the results of the ground-state energy using quantum simulation based on pseudo-imaginary-time evolution. The parameters used for the calculations are detailed in Sec. 5.2.4. To ensure a fair comparison, the number of samples in the Monte Carlo method was set to match the number of evaluation points denoted as N^{TCI} obtained using the proposed method. The average number of evaluation points for the numerator and denominator were rounded up to the nearest decimal and set as \bar{N}_n^{TCI} and \bar{N}_d^{TCI} , respectively. The Monte Carlo sampling numbers for the numerator and denominator were set as $N_n^{\text{MC}} = \bar{N}_n^{\text{TCI}}$ and $N_d^{\text{MC}} = \bar{N}_d^{\text{TCI}}$. For different system sizes, the pairs $(n_{\text{site}}, \bar{N}_n^{\text{TCI}}, \bar{N}_d^{\text{TCI}})$ were set as $(2, 767, 742)$, $(4, 1793, 1732)$, and $(6, 4480, 4592)$.

Figure 6(a) shows the relative error and its distribution of the ground-state energy calculated using three methods: the Monte Carlo method, the QTCI method, and the proposed method. These calculations were performed 20 times for each method and system sizes $n_{\text{site}} = 2, 4, 6$. When comparing the relative error in the expected value of the Hamiltonian, the proposed method produces results that are nearer to the exact ground-state energy and show less variation than the other approaches.

Figure 6(b) compares the E_0 dependency of the real part of the $\langle \tilde{H} \rangle_{G_T}(\beta)$ calculated using the QTCI method and the proposed method. The proposed method outperforms QTCI in accurately and consistently determining the E_0 dependency under noisy conditions, using a comparable number of samples.

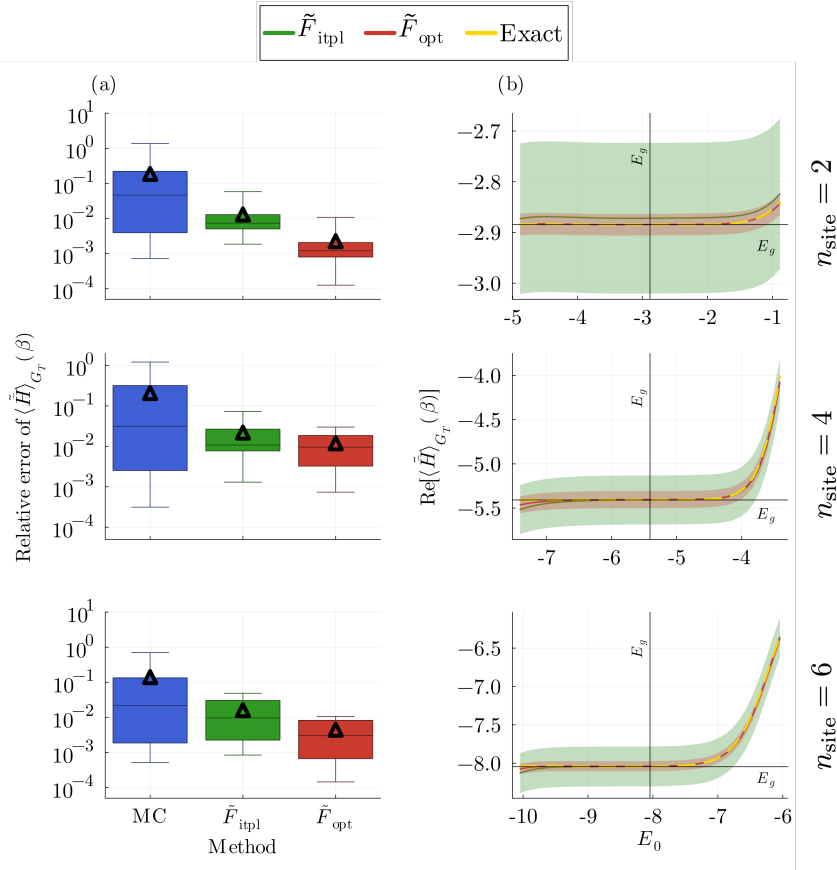


Figure 6: Results for the relative error of the ground-state energy computed by exact diagonalization method and each scheme (a) and E_0 dependency of the real part of the $\langle \tilde{H} \rangle_{G_T}(\beta)$ (b). Here, we compute its variation over 20 calculations using each scheme, with each different random seed. The triangle markers in (a) and the solid line in (b) represent the mean values, and the shading indicates the variance. The parameter set used for implementation is presented in Sec. 5.2.4. Due to the high variance of the Monte Carlo results, they are omitted from Fig. 6(b).

6 Conclusion

We propose a method to optimize TTs for functions subject to random noise in their evaluations. Here, we optimize an initial guess of TT by fitting it to measured points obtained from TCI. These measured points served as fitting points appropriately by capturing the overall structure of the target functions. As a result, we get the optimized TT that accurately approximates the noise-free function. We used QTCI in the proposed method and applied it to the sine function with added Gaussian noise and two-time correlation functions computed by quantum computers. Our approach resulted in a high-precision QTT compared to the QTCI method. Furthermore, we applied the optimized TTs of two-time correlation functions to quantum simulations based on pseudo-imaginary-time evolution for ground-state energy calculations. Our method achieved higher precision in determining the ground-state energy compared to the QTCI and Monte Carlo methods. Our study shows that the proposed method robustly learns TTs from functions under the influence of random noise in function evaluations.

We have several future directions. We aim to improve the accuracy of our proposed

method by incorporating L1 regularization and smoothness conditions into the cost function during optimization. Additionally, combining the denoising techniques based on the Fourier transform proposed in [33] with our method may further enhance the denoising of QTT. Also, it may be possible to suppress the effect of noise in the correlation functions by incorporating the weight of $g(t)g(t')$ into the optimization process in the quantum simulation. We consider extending its application to compute imaginary-time Green's functions [34–36] based on pseudo-imaginary-time evolution, which poses challenges. Finally, this approach may also find other applications, such as quantum state tomography for photonic quantum computing [37].

Acknowledgements

We are grateful to Marc K. Ritter and Jan von Delft for providing early access to the `TensorCrossInterpolation.jl` for TCI [27]. R. S. was supported by the JSPS KAKENHI Grant No. 23KJ0295. H. S. was supported by JSPS KAKENHI Grants No. 21H01041, No. 21H01003, and No. 23H03817 as well as JST PRESTO Grant No. JPMJPR2012 and JST FOREST Grant No. JPMJFR2232, Japan. This work was supported by Institute of Mathematics for Industry, Joint Usage/Research Center in Kyushu University. (FY2023 CATEGORY “Use of Julia in Mathematics and Physics” (2023a015).)

A Element-wise multiplication and integration with tensor trains

A.1 Element-wise multiplication

In this section, we consider computing $C(t)$ via the element-wise multiplication of functions $A(t)$ and $B(t)$:

$$C(t) = A(t) \cdot B(t). \quad (31)$$

In tensor network notation, this element-wise multiplication can be defined as:

$$C(t_1, t_2, \dots, t_{\mathcal{R}}) = A(t_1, t_2, \dots, t_{\mathcal{R}}) \cdot B(t_1, t_2, \dots, t_{\mathcal{R}}). \quad (32)$$

This operation corresponds to specifying certain indices of tensor C and assigning the corresponding element-wise multiplied values of tensors A and B to the indices in tensor C .

The functions $A(t)$, $B(t)$, and $C(t)$ can be represented in the TT. Specifically, $A(t)$ and $B(t)$ are expressed as \mathcal{R} -order TTs as follows:

$$A_{t_1 t_2 \dots t_{\mathcal{R}}} \approx \sum_{\alpha_1=1}^{\chi_1^A} \cdots \sum_{\alpha_{\mathcal{R}-1}=1}^{\chi_{\mathcal{R}-1}^A} [A_1]_{1\alpha_1}^{t_1} \cdots [A_{\mathcal{R}}]_{\alpha_{\mathcal{R}-1}1}^{t_{\mathcal{R}}}, \quad (33)$$

$$B_{t_1 t_2 \dots t_{\mathcal{R}}} \approx \sum_{\beta_1=1}^{\chi_1^B} \cdots \sum_{\beta_{\mathcal{R}-1}=1}^{\chi_{\mathcal{R}-1}^B} [B_1]_{1\beta_1}^{t_1} \cdots [B_{\mathcal{R}}]_{\beta_{\mathcal{R}-1}1}^{t_{\mathcal{R}}}. \quad (34)$$

To represent the element-wise multiplication $A(t) \cdot B(t)$ in MPO and TT, we use a delta function to express $A(t)$ as an MPO. The local bond indices t_i and t'_i with the same

length scale are diagonalized using the delta function:

$$A_{t_1 t_2 \dots t_{\mathcal{R}}}^{t'_1 t'_2 \dots t'_{\mathcal{R}}} \approx \sum_{\alpha_1=1}^{\chi_1^A} \dots \sum_{\alpha_{\mathcal{R}-1}=1}^{\chi_{\mathcal{R}-1}^A} [A_1]_{1\alpha_1}^{t_1 t'_1} \dots [A_{\mathcal{R}}]_{\alpha_{\mathcal{R}-1} 1}^{t_{\mathcal{R}} t'_{\mathcal{R}}}, \quad (35)$$

$$[A_k]_{\alpha_{j-1} \alpha_j}^{t_j t'_j} = [A_k]_{\alpha_{j-1} \alpha_j}^{t_j} \delta_{t_j, t'_j} \quad (k \in 1, \dots, \mathcal{R}). \quad (36)$$

By expressing A in the MPO representation, the element-wise multiplication $A(t) \cdot B(t)$ can be calculated through the contraction of MPO and TT. The element-wise multiplication diagram is shown in Fig. 7. If the bond dimensions of tensors A and B are denoted as χ_A and χ_B , respectively, the computational complexity is $\mathcal{O}(\mathcal{R} \chi_A^2 \chi_B^2)$.

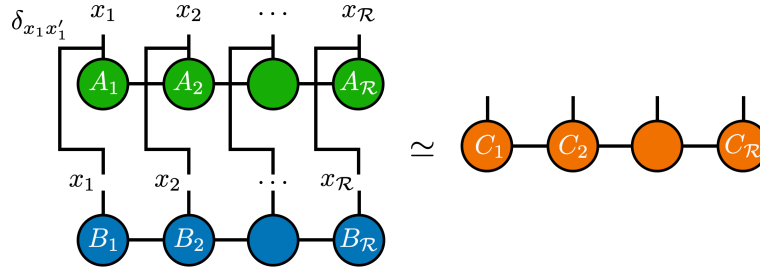


Figure 7: Diagram of the element-wise multiplication. The approximation means that the resulting TT is compressed by using SVD.

A.2 Integration

We consider the QTT, \tilde{F} of \mathcal{L} -order with a local dimension $d = 2$ and bond dimension χ , of a function $f(x)$. The sum of the function $f(x)$ values at grid points with intervals of $\Delta x = 1/2^{\mathcal{L}}$ is equivalent to the Riemann sum, as follows:

$$\int_{x_0}^{x_{2^{\mathcal{L}}-1}} f(x) dx \approx \sum_{i=0}^{2^{\mathcal{L}}-1} f(x_i) \Delta x. \quad (37)$$

The element-wise sum operation, multiplied by Δx , is equivalent to contracting the QTT of $f(x)$ with the following equation:

$$I(\sigma_1, \dots, \sigma_{\mathcal{L}}) = \Delta x \begin{bmatrix} 1 \\ 1 \end{bmatrix} \otimes \begin{bmatrix} 1 \\ 1 \end{bmatrix} \otimes \dots \otimes \begin{bmatrix} 1 \\ 1 \end{bmatrix}. \quad (38)$$

The integration operation in QTT can be computed by contracting \tilde{F} with tensors of bond dimension 1 filled with ones for each core tensor of the QTT. This can be extended to multivariate functions. Diagrammatically, it can be represented as follows:

$$\sum_{\sigma_1, \dots, \sigma_{\mathcal{L}}}^d \left\{ \sum_{i_1, \dots, i_{\mathcal{L}-1}}^{\chi} [F_1]_{1i_1}^{\sigma_1} [F_2]_{i_1 i_2}^{\sigma_2} \dots [F_{\mathcal{L}}]_{i_{\mathcal{L}-1} 1}^{\sigma_{\mathcal{L}}} \right\} \iff \left\{ \begin{array}{c} \bullet \text{---} \bullet \text{---} \dots \text{---} \bullet \\ | \quad | \quad \quad \quad | \\ \bullet \quad \bullet \quad \quad \quad \bullet \end{array} \right\} d. \quad (39)$$

where the computational complexity is $\mathcal{O}(\mathcal{L} \chi^2)$.

B Calculating the real-time correlation function $\langle O \rangle(t, t')$

The real-time correlation function $\langle O \rangle(t, t')$ can be rewritten as shown in Eq. (40):

$$\begin{aligned} \langle O \rangle(t, t') &= \langle \Psi(0) | e^{iHt'} O e^{-iHt} | \Psi(0) \rangle \\ &= e^{iE_0(t-t')} \langle \Psi(0) | e^{i\bar{H}t'} O e^{-i\bar{H}t} | \Psi(0) \rangle \\ &= e^{iE_0(t-t')} \overline{\langle O \rangle}(t, t'). \end{aligned} \quad (40)$$

The quantum circuit required for calculating $\overline{\langle O \rangle}(t, t')$ is shown in Fig. 8.

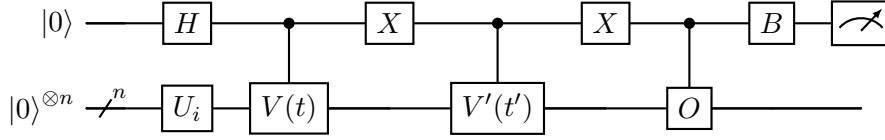


Figure 8: Quantum circuit for calculating $\overline{\langle O \rangle}(t, t')$. Here, we denote unitary operators $V(t) = e^{-i\bar{H}t}$, $V'(t') = e^{-i\bar{H}t'}$, and $U_i = H^{\otimes n}$, along with the unitary physical quantity O . Additionally, the B gate is set to $B = H$ (Pauli- X measurement) for calculating the real part of $\overline{\langle O \rangle}(t, t')$, and $B = HS^\dagger$ (Pauli- Y measurement) for calculating the imaginary part.

Following the circuit in Fig. 8, the computation proceeds as follows:

$$\begin{aligned} &|0\rangle \otimes |0\rangle^{\otimes n} \\ &\xrightarrow{H \otimes U_i} \frac{1}{\sqrt{2}} (|0\rangle + |1\rangle) \otimes |\Psi(0)\rangle \\ &\xrightarrow{|0\rangle\langle 0| \otimes I^{\otimes n} + |1\rangle\langle 1| \otimes V(t)} \frac{1}{\sqrt{2}} \{ |0\rangle \otimes |\Psi(0)\rangle + |1\rangle \otimes V(t) |\Psi(0)\rangle \} \\ &\xrightarrow{X \otimes I^{\otimes n}} \frac{1}{\sqrt{2}} \{ |1\rangle \otimes |\Psi(0)\rangle + |0\rangle \otimes V(t) |\Psi(0)\rangle \} \\ &\xrightarrow{|0\rangle\langle 0| \otimes I^{\otimes n} + |1\rangle\langle 1| \otimes V'(t')} \frac{1}{\sqrt{2}} \{ |1\rangle \otimes V'(t') |\Psi(0)\rangle + |0\rangle \otimes V(t) |\Psi(0)\rangle \} \\ &\xrightarrow{X \otimes I^{\otimes n}} \frac{1}{\sqrt{2}} \{ |0\rangle \otimes V'(t') |\Psi(0)\rangle + |1\rangle \otimes V(t) |\Psi(0)\rangle \} \\ &\xrightarrow{|0\rangle\langle 0| \otimes I^{\otimes n} + |1\rangle\langle 1| \otimes O} \frac{1}{\sqrt{2}} \{ |0\rangle \otimes V'(t') |\Psi(0)\rangle + |1\rangle \otimes OV(t) |\Psi(0)\rangle \}. \end{aligned} \quad (41)$$

To calculate the real part of $\overline{\langle O \rangle}(t, t')$, the B gate is set to H (Pauli- X measurement). For the imaginary-time part, the gate is set to HS^\dagger (Pauli- Y measurement). For $\overline{\langle O \rangle}(t, t') = \langle \Psi(0) | V'^{\dagger}(t') O V(t) | \Psi(0) \rangle \equiv a + ib$ ($a, b \in \mathbb{R}$), we can proceed with the computation for Pauli- X measurement and Pauli- Y measurement case, respectively.

For the case of Pauli- X measurement, the equation in Eq. (41) is transformed as follows:

$$\begin{aligned} &\xrightarrow{H \otimes I^{\otimes n}} \frac{1}{\sqrt{2}} \left\{ \frac{1}{\sqrt{2}} (|0\rangle + |1\rangle) \otimes V'(t') |\Psi(0)\rangle + \frac{1}{\sqrt{2}} (|0\rangle - |1\rangle) \otimes OV(t) |\Psi(0)\rangle \right\} \\ &= \frac{1}{2} \left[|0\rangle \otimes \{ V'(t') |\Psi(0)\rangle + OV(t) |\Psi(0)\rangle \} + |1\rangle \otimes \{ V'(t') |\Psi(0)\rangle - OV(t) |\Psi(0)\rangle \} \right], \end{aligned} \quad (42)$$

The probability of measuring the first qubit as 0, denoted as P_{x0} , can be computed as follows:

$$\begin{aligned}
P_{x0} &= \left| \frac{V'(t') |\Psi(0)\rangle + OV(t) |\Psi(0)\rangle}{2} \right|^2 \\
&= \frac{1}{4} \{ \langle \Psi(0) | V'^{\dagger}(t') + \langle \Psi(0) | V^{\dagger}(t) O^{\dagger} \} \{ V'(t') |\Psi(0)\rangle + OV(t) |\Psi(0)\rangle \} \\
&= \frac{1+a}{2},
\end{aligned} \tag{43}$$

The probability of measuring the first qubit as 1, denoted as P_{x1} , can be computed as follows:

$$\begin{aligned}
P_{x1} &= \left| \frac{V'(t') |\Psi(0)\rangle - OV(t) |\Psi(0)\rangle}{2} \right|^2 \\
&= \frac{1}{4} \{ \langle \Psi(0) | V'^{\dagger}(t') - \langle \Psi(0) | V^{\dagger}(t) O^{\dagger} \} \{ V'(t') |\Psi(0)\rangle - OV(t) |\Psi(0)\rangle \} \\
&= \frac{1-a}{2},
\end{aligned} \tag{44}$$

Thus, the expectation value from the Pauli-X measurement is

$$\langle Z \rangle = (+1) \times P_{x0} + (-1) \times P_{x1} = a, \tag{45}$$

For the case of Pauli-Y measurement, the equation in Eq. (41) is transformed as follows:

$$\begin{aligned}
&\xrightarrow{HS^{\dagger} \otimes I^{\otimes n}} \frac{1}{\sqrt{2}} \left\{ \frac{1}{\sqrt{2}} (|0\rangle + |1\rangle) \otimes V'(t') |\Psi(0)\rangle - i \frac{1}{\sqrt{2}} (|0\rangle - |1\rangle) \otimes OV(t) |\Psi(0)\rangle \right\} \\
&= \frac{1}{2} \left[|0\rangle \otimes \{ V'(t') |\Psi(0)\rangle - iOV(t) |\Psi(0)\rangle \} + |1\rangle \otimes \{ V'(t') |\Psi(0)\rangle + iOV(t) |\Psi(0)\rangle \} \right],
\end{aligned} \tag{46}$$

The probability of measuring the first qubit as 0, denoted as P_{y0} , can be computed as follows:

$$\begin{aligned}
P_{y0} &= \left| \frac{V'(t') |\Psi(0)\rangle - iOV(t) |\Psi(0)\rangle}{2} \right|^2 \\
&= \frac{1}{4} \{ \langle \Psi(0) | V'^{\dagger}(t') + i \langle \Psi(0) | V^{\dagger}(t) O^{\dagger} \} \{ V'(t') |\Psi(0)\rangle - iOV(t) |\Psi(0)\rangle \} \\
&= \frac{1+b}{2},
\end{aligned} \tag{47}$$

The probability of measuring the first qubit as 1, denoted as P_{y1} , can be computed as follows:

$$\begin{aligned}
P_{y1} &= \left| \frac{V'(t') |\Psi(0)\rangle + iOV(t) |\Psi(0)\rangle}{2} \right|^2 \\
&= \frac{1}{4} \{ \langle \Psi(0) | V'^{\dagger}(t') - i \langle \Psi(0) | V^{\dagger}(t) O^{\dagger} \} \{ V'(t') |\Psi(0)\rangle + iOV(t) |\Psi(0)\rangle \} \\
&= \frac{1-b}{2},
\end{aligned} \tag{48}$$

Thus, the expectation value from the Pauli-Y measurement is:

$$\langle Z \rangle = (+1) \times P_{y0} + (-1) \times P_{y1} = b, \tag{49}$$

Thus, we can calculate the real-time correlation function $\langle O \rangle(t, t')$ by separating $\overline{\langle O \rangle}(t, t')$ into its real and imaginary parts. In this calculation, shot noise resulting from a finite number of measurements and Trotter errors due to the limited number of Trotter steps is included.

C Bond dimensions of two-time correlation functions without noise

We compute each element of the two-time correlation function using state vector simulation without noise, i.e., shot noise and Trotter error, and determine the bond dimension by compressing this correlation function using SVD.

Figure 9(a) shows the shape of the real-time correlation functions $\overline{\langle \bar{H} \rangle}(t, t')$ and $\overline{\langle \bar{1} \rangle}(t, t')$, calculated without shot noise and Trotter errors, over the interval $t, t' \in [-2, 2]$. The upper panel displays the real and imaginary parts of the correlation function $\overline{\langle \bar{H} \rangle}(t, t')$ used for calculating the numerator of $\langle \bar{H} \rangle_{G_T}(\beta)$, while the lower panel shows those of the correlation function $\overline{\langle \bar{1} \rangle}(t, t')$ used for the denominator. Here, the parameters are set to $\lambda = 1.2$, $n_{\text{site}} = 4$ and $\mathcal{R} = 8$. The two-time correlation functions exhibit a characteristic wave-like striped pattern along the 45-degree direction.

Figure 9(b) shows that the correlation function exhibits a low-rank structure. The maximum bond dimensions reach only around 12 for system sizes n_{site} up to 8 sites.

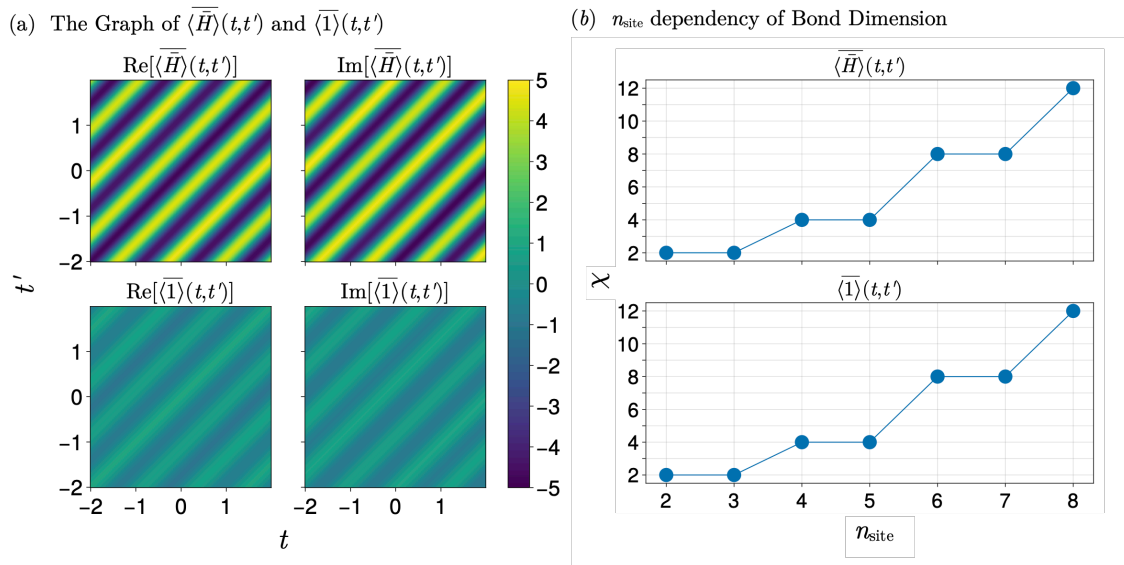


Figure 9: Computed correlation functions using state-vector simulation without shot noise, Trotter error (a), and their maximum bond dimensions (b). The QTT was constructed using SVD, setting its tolerance 10^{-10} .

References

- [1] J. I. Latorre, [Image compression and entanglement](#) (2005), [quant-ph/0510031](#).
- [2] K. Sozykin, A. Chertkov, R. Schutski, A.-H. Phan, A. Cichocki and I. Oseledets, [Ttopt: A maximum volume quantized tensor train-based optimization and its application to reinforcement learning](#) (2022), [2205.00293](#).
- [3] E. Stoudenmire and D. J. Schwab, [Supervised learning with tensor networks](#), In D. Lee, M. Sugiyama, U. Luxburg, I. Guyon and R. Garnett, eds., [Advances in Neural Information Processing Systems](#), vol. 29. Curran Associates, Inc. (2016).

- [4] N. Gourianov, M. Lubasch, S. Dolgov, Q. Y. van den Berg, H. Babaei, P. Givi, M. Kiffner and D. Jaksch, A quantum-inspired approach to exploit turbulence structures, *Nature Computational Science* **2**(1), 30–37 (2022), doi:10.1038/s43588-021-00181-1.
- [5] E. Ye and N. F. G. Loureiro, Quantum-inspired method for solving the vlasov-poisson equations, *Phys. Rev. E* **106**, 035208 (2022), doi:10.1103/PhysRevE.106.035208.
- [6] E. Ye and N. Loureiro, Quantized tensor networks for solving the vlasov-maxwell equations (2024), 2311.07756.
- [7] E. Kornev, S. Dolgov, K. Pinto, M. Pflitsch, M. Perelshtein and A. Melnikov, Numerical solution of the incompressible navier-stokes equations for chemical mixers via quantum-inspired tensor train finite element method (2023), 2305.10784.
- [8] S. Dolgov and B. Khoromskij, Simultaneous state-time approximation of the chemical master equation using tensor product formats, *Numerical Linear Algebra with Applications* **22**(2), 197 (2015), doi:https://doi.org/10.1002/nla.1942, https://onlinelibrary.wiley.com/doi/pdf/10.1002/nla.1942.
- [9] H. Shinaoka, M. Wallerberger, Y. Murakami, K. Nogaki, R. Sakurai, P. Werner and A. Kauch, Multiscale space-time ansatz for correlation functions of quantum systems based on quantics tensor trains, *Physical Review X* **13**(2) (2023), doi:10.1103/physrevx.13.021015.
- [10] Y. Núñez Fernández, M. Jeannin, P. T. Dumitrescu, T. Kloss, J. Kaye, O. Parcollet and X. Waintal, Learning feynman diagrams with tensor trains, *Phys. Rev. X* **12**, 041018 (2022), doi:10.1103/PhysRevX.12.041018.
- [11] H. Takahashi, R. Sakurai and H. Shinaoka, Compactness of quantics tensor train representations of local imaginary-time propagators (2024), 2403.09161.
- [12] M. Kastoryano and N. Pancotti, A highly efficient tensor network algorithm for multi-asset fourier options pricing (2022), 2203.02804.
- [13] R. Sakurai, H. Takahashi and K. Miyamoto, Learning parameter dependence for fourier-based option pricing with tensor networks (2024), 2405.00701.
- [14] I. Oseledets and E. Tyrtyshnikov, Tt-cross approximation for multidimensional arrays, *Linear Algebra and its Applications* **432**(1), 70 (2010), doi:https://doi.org/10.1016/j.laa.2009.07.024.
- [15] M. Bebendorf, Adaptive Cross Approximation of Multivariate Functions, *Constructive Approximation* **34**(2), 149 (2011), doi:10.1007/s00365-010-9103-x.
- [16] Z. Qin, A. Lidiak, Z. Gong, G. Tang, M. B. Wakin and Z. Zhu, Error analysis of tensor-train cross approximation (2023), 2207.04327.
- [17] A. Lidiak, C. Jameson, Z. Qin, G. Tang, M. B. Wakin, Z. Zhu and Z. Gong, Quantum state tomography with tensor train cross approximation (2022), 2207.06397.
- [18] M. K. Ritter, Y. Núñez Fernández, M. Wallerberger, J. von Delft, H. Shinaoka and X. Waintal, Quantics tensor cross interpolation for high-resolution parsimonious representations of multivariate functions, *Phys. Rev. Lett.* **132**, 056501 (2024), doi:10.1103/PhysRevLett.132.056501.

- [19] I. V. Oseledets, Approximation of matrices with logarithmic number of parameters, Doklady Math. **80**(2), 653 (2009), doi:10.1134/S1064562409050056.
- [20] B. N. Khoromskij, $O(d \log N)$ -quantics approximation of n-d tensors in high-dimensional numerical modeling, Constr. Approx. **34**(2), 257 (2011), doi:10.1007/s00365-011-9131-1.
- [21] B. N. Khoromskij, Tensor Numerical Methods in Scientific Computing, vol. 19 of Radon Series on Computational and Applied Mathematics, De Gruyter, Berlin, Boston, first edn. (2018).
- [22] U. Schollwock, The density-matrix renormalization group in the age of matrix product states, Ann. Phys. **326**(1), 96 (2011), doi:10.1016/j.aop.2010.09.012.
- [23] M. Huo and Y. Li, Error-resilient Monte Carlo quantum simulation of imaginary time, Quantum **7**, 916 (2023), doi:10.22331/q-2023-02-09-916.
- [24] S.-N. Sun, M. Motta, R. N. Tazhigulov, A. T. Tan, G. K.-L. Chan and A. J. Minnich, Quantum computation of finite-temperature static and dynamical properties of spin systems using quantum imaginary time evolution, PRX Quantum **2**, 010317 (2021), doi:10.1103/PRXQuantum.2.010317.
- [25] T. Kosugi, Y. Nishiyama, H. Nishi and Y.-i. Matsushita, Imaginary-time evolution using forward and backward real-time evolution with a single ancilla: First-quantized eigensolver algorithm for quantum chemistry, Phys. Rev. Res. **4**, 033121 (2022), doi:10.1103/PhysRevResearch.4.033121.
- [26] S. McArdle, T. Jones, S. Endo, Y. Li, S. C. Benjamin and X. Yuan, Variational ansatz-based quantum simulation of imaginary time evolution, npj Quantum Information **5**(1) (2019), doi:10.1038/s41534-019-0187-2.
- [27] Y. Núñez Fernández, M. K. Ritter, M. Jeannin, J.-W. Li, T. Kloss, O. Parcollet, J. von Delft, H. Shinaoka and X. Waintal, In preparation (2024).
- [28] M. Fishman, S. R. White and E. M. Stoudenmire, The ITensor Software Library for Tensor Network Calculations, SciPost Phys. Codebases p. 4 (2022), doi:10.21468/SciPostPhysCodeb.4.
- [29] AtelierArith, Kyulacs.jl: Julia interface for Qulacs (2024).
- [30] Y. Suzuki, Y. Kawase, Y. Masumura, Y. Hiraga, M. Nakadai, J. Chen, K. M. Nakanishi, K. Mitarai, R. Imai, S. Tamiya, T. Yamamoto, T. Yan et al., Qulacs: a fast and versatile quantum circuit simulator for research purpose, Quantum **5**, 559 (2021), doi:10.22331/q-2021-10-06-559.
- [31] P. K. Mogensen and A. N. Riseth, Optim: A mathematical optimization package for Julia, Journal of Open Source Software **3**(24), 615 (2018), doi:10.21105/joss.00615.
- [32] M. Innes, Don't unroll adjoint: Differentiating ssa-form programs, CoRR **abs/1810.07951** (2018), 1810.07951.
- [33] A. Chertock, C. Leonard, S. Tsynkov and S. Utyuzhnikov, Denoising convolution algorithms and applications to sar signal processing (2023), 2301.13339.

- [34] R. Sakurai, O. J. Backhouse, G. H. Booth, W. Mizukami and H. Shinaoka, Comparative study on compact quantum circuits of hybrid quantum-classical algorithms for quantum impurity models, Phys. Rev. Res. **6**, 023110 (2024), doi:10.1103/PhysRevResearch.6.023110.
- [35] R. Sakurai, W. Mizukami and H. Shinaoka, Hybrid quantum-classical algorithm for computing imaginary-time correlation functions, Phys. Rev. Res. **4**, 023219 (2022), doi:10.1103/PhysRevResearch.4.023219.
- [36] H. Chen, M. Nusspickel, J. Tilly and G. H. Booth, Variational quantum eigensolver for dynamic correlation functions, Phys. Rev. A **104**, 032405 (2021), doi:10.1103/PhysRevA.104.032405.
- [37] A. I. Lvovsky and M. G. Raymer, Continuous-variable optical quantum-state tomography, Reviews of Modern Physics **81**(1), 299–332 (2009), doi:10.1103/revmodphys.81.299.